

Platelet adhesion, aggregation, and embolism on artificial surfaces in non-parallel blood flow

Thorsten Kragh · Jens Schaller · Ulrich Kertzscher · Klaus Affeld · Armin Reininger · Michael Spannagl

Received: 29 July 2014 / Accepted: 31 January 2015 / Published online: 13 February 2015
© Springer-Verlag Berlin Heidelberg 2015

Abstract When using artificial surfaces that come into contact with the bloodstream, it is important to consider the undesirable consequences of thrombus formation and embolization. Although great progress has been made by creating new surfaces and antithrombotic coatings or evaluating flow conditions, unexpected platelet adhesion and aggregation can lead to the sudden formation of an adverse thrombus. Our experiments in a stagnation point flow chamber with citrate-anticoagulated whole blood and ADP-stimulated platelets mimicked the situations of implanted artificial organs, e.g., mechanical circulatory support devices, or extravascular circulation. With video microscopy, real-time platelet characteristics were observed at shear rate levels between 50 and 500 s⁻¹ on glass, von Willebrand factor, and polyurethane surfaces for at least 5 min after the first contact. Platelet adhesion and aggregation were observed with distinctness in aggregate size, surface coverage, aggregate size, probability of an embolic event, and platelet contraction. The probability of an embolic event increased at lower flow rates. Additionally,

platelet contraction was affected by the flow rate. Raising the flow rate intensified the platelet contraction. With this setup, the microembolization caused by surface contact and flow and platelet contraction can be detected in a real-time direct observation. This capability addresses both technical and clinical issues, such as thrombus and embolus formation, and may improve the research on the hemocompatibility of biomaterials.

Keywords Stagnation point flow · Platelet contraction · Carbothane · Pellethane · Hemocompatibility · Flow chamber

Abbreviations

ADP	Adenosine diphosphate
BSA	Bovine serum albumin
CFD	Computational fluid dynamics
KCl	Potassium chloride
MCSD	Mechanical circulatory support devices
NaCl	Sodium chloride
NaH ₂ PO ₄	Sodium dihydrogen phosphate
PBS	Phosphate-buffered saline
PPACK	H-D-Phe-Pro-Arg-chloromethylketone trifluoroacetate
PRP	Platelet-rich plasma
VWF	von Willebrand factor

Electronic supplementary material The online version of this article (doi:10.1007/s10404-015-1557-5) contains supplementary material, which is available to authorized users.

T. Kragh (✉) · M. Spannagl
Department of Transfusion Medicine, Cell Therapeutics and Hemostasis, Medical Center of the University of Munich, Ziemssenstraße 1, 80336 Munich, Germany
e-mail: thorsten.kragh@med.uni-muenchen.de

J. Schaller · U. Kertzscher · K. Affeld
Biofluid Mechanics Laboratory, Charité-Universitätsmedizin Berlin, Berlin, Germany

A. Reininger
Baxter Innovations GmbH, Vienna, Austria

1 Introduction

Implanted medical devices and devices attached to the cardiovascular system contact blood. Several blood components may deposit on the contact surface. Depending on the surface, proteins adhere and support the adherence of platelets, often leading to thrombus formation. In most

cases, these formations are not desirable because they can lead to the malfunction of the bearings of heart pumps or the closure of stented vessels. Furthermore, a larger thrombus may detach and will interrupt the blood flow of smaller downstream vessels. When this occurs in the brain, a patient will suffer a stroke. In ventricular assist devices, approximately 0.74 strokes per patient year occur (Backes et al. 2012); thus, this is a major issue for such devices (Ratner 2007). The flow with its wall shear stress is one critical factor in this formation process (Hathcock 2006). The other factor is the material (Claesson et al. 1995). The most used materials in medicine are polymers (polyurethanes, silicones) and metals (titanium, stainless steels). Polyurethanes are widely used for blood contact surfaces, such as intra-aortic balloons (Vermette et al. 2001), blood pumps (Beiras-Fernandez et al. 2013), heart valves (Kuetting et al. 2011), or stent coatings (Trigwell et al. 2006). To improve the hemocompatibility, surface modifications with heparin or antiprotein-adsorbing sugar residues have been developed (Heise et al. 2006). Furthermore, for a better understanding of the mechanisms, the adsorption kinetics of different thrombotic plasma proteins, including fibrinogen, von Willebrand factor (VWF), and factor XI, to plastic polymers have been tested (Horbett 1993). Depending on surface properties such as the charge or sugar residues, certain proteins may be initially adsorbed but are exchanged by other proteins after some time due to the Vroman effect (Hirsh et al. 2013). Additionally, some proteins are hemostatically inactivated or activated through conformational changes in their active platelet binding domains via the process of adsorption. Thus, the mere presence or absence of proteins on a particular surface does not necessarily determine its thrombogenicity (Jung et al. 2013), and the direct observation of the reactivity of platelets with an artificial surface is accordingly very important for the classification of its hemostatic properties (Reininger et al. 2000; Schaller et al. 2013). Many types of polyurethane and other plastic materials have been introduced and tested for blood biocompatibility, but the measurements were taken either in static systems with chemically fixed samples (Fare et al. 2005; Handa et al. 2014) or in circular flow devices (Chandler loop) that reuse the same blood, sometimes for hours (Krajewski et al. 2014). Repeatedly, circulating the material may lead to enhanced platelet activation due to pumping and contact with the surfaces (van Oeveren et al. 2012). Microfluidic devices have the advantage of requiring smaller amounts of blood to avoid recirculation when studying thrombus formation. Colace et al. listed the applications of these devices. The main aspects are the impact of flow and different agonists on platelet adherence and aggregation. Furthermore, the translocation and rolling of blood cells are current research areas. For that

purpose, blood is guided through various channels and stenotic geometries to induce shear gradients that should better represent the *in vivo* situation (Colace et al. 2013; Neeves et al. 2013; Westein et al. 2012).

Physiologically, different factors lead to platelet activation—shear stress, surface-bound-specific (e.g., collagen) or non-specific (e.g., artificial surfaces) platelet receptor interactions, or platelet agonists, such as adenosine diphosphate (ADP), thromboxane, or thrombin. A slight stimulation with ADP or light shear stresses can be reversible, and the platelets may go back to a resting state when not further stimulated. Nevertheless, the receptors for fibrinogen (integrin $\alpha_2\beta_3$) are activated on the platelet surface, causing adhesion to fibrinogen and VWF. After activation platelets aggregate, start shape change and secrete stored agonists from α -granules. Additional platelet recruitment, activation and hence aggregation at the site is promoted by agonists. Plasma proteins, such as fibrinogen and VWF, serve as the glue between platelets and stabilize the growing thrombus (Versteeg et al. 2013).

In the present work, we used real-time fluorescence video-microscopy for direct observations to characterize the adhesion, aggregation, embolization, and contraction processes of platelets on different surfaces exposed to three flow conditions using a stagnation point flow chamber to create a non-parallel flow situation. Then, we studied the effect on these processes. The blood only contacted with the surface material and the flow situation once.

2 Materials and methods

2.1 Fluid and surface preparation

Blood from 21 healthy human volunteers was drawn from an antecubital vein and collected in citrate S-Monovettes[®] (sodium citrate: final concentration 10.6 mM; Sarstedt AG&Co, Nümbrecht, Germany). The first 3 ml of drawn blood was discarded to prevent uncontrolled platelet activation. The platelet-rich plasma (PRP) was separated from the blood cells by centrifugation ($120\times g$ for 20 min) at room temperature. For epifluorescence microscopy, the platelets in the PRP were incubated for 1 h with calcein red–orange AM (10 $\mu\text{g}/\text{ml}$ PRP; Life Technologies GmbH, Darmstadt, Germany) in the dark at room temperature. Prior to the flow experiments, the blood cells and PRP were combined to obtain a physiological hematocrit (38–43 %) and platelet count (180,000–390,000/ μl) using a Sysmex KX-21 (Sysmex Deutschland GmbH, Norderstedt, Germany). The donors did not take any medication that can affect platelets, such as aspirin, for at least 14 days. All studies involving human subjects were conducted in accordance with the Declaration of Helsinki and were approved by the

Ethics Commission of the Ludwig-Maximilians-University Munich. The withdrawal of human blood took place at the Clinic for Anesthesiology, Department of Transfusion Medicine in Munich. Informed consent was obtained from all subjects prior to participation in the study.

To clarify the involvement of plasma proteins in platelet adhesion and aggregation, additional experiments with washed blood cell suspensions were performed. The citrate-anticoagulated whole blood was centrifuged ($1,400\times g$ for 13 min at room temperature), and the supernatant plasma was discarded. The platelet and leukocyte cushion that sedimented on top of the erythrocytes was pipetted and resuspended with an equivalent volume of divalent cation-free Hepes/Tyrode buffer [17 mM Hepes (*N*-2-hydroxyethyl piperazine-*N'*-2-ethanesulfonic acid), 130 mM NaCl, 2.7 mM KCl, 0.4 mM NaH_2PO_4 , and 2.8 mM dextrose] at pH 6.5. H-D-Phe-Pro-Arg-chloromethylketone trifluoroacetate salt (PPACK; final concentration: 46 μM ; Bachem Bioscience, King of Prussia, PA) was added to the blood where indicated to inhibit thrombin-induced fibrin formation. This procedure was repeated twice, but no PPACK was added after the last washing step; the buffy coat was removed for calcein staining as described above. To adjust the platelet count and hematocrit to physiological levels, the cell fraction was resuspended in Hepes/Tyrode buffer, pH 7.4, containing 50 mg/ml bovine serum albumin (BSA; Sigma-Aldrich Chemie). Divalent cations were reconstituted before the experiment (final concentration: CaCl_2 0.6 mM, MgCl_2 0.3 mM).

Glass coverslips were coated with Haemate[®] P 500 solution (1 unit active protein/ml; CSL Behring GmbH, Hattersheim am Main, Germany) for 1 h to obtain homogeneous VWF absorption on the surface (Ruggeri et al. 2006). The coverslips were also coated with thin layers of two different

polyurethanes, Carbothane and Pellethane (Arjun and Ramesh 2012; Shin et al. 2012); untreated glass cover slips were used as the reference, as described elsewhere (Reininger et al. 2000). For every condition, at least 16 flow experiments were performed.

2.2 Experimental setup and data acquisition

The flow chamber (Fig. 1a; inlet diameter 650 μm , chamber height 480 μm) was loaded with a cover slip, filled with phosphate-buffered saline (PBS), and mounted onto a motorized stage of an inverse, epifluorescence, temperature-controlled microscope (Eclipse TE2000-E; Nikon, Düsseldorf, Germany). For a characterization of the flow field, computational fluid dynamics (CFD) simulations were performed using the flow solver Fluent 6.2.3 (Fluent Inc, Canonsburg, USA) under the assumption of laminar flow. For that purpose, a three-dimensional mesh was generated for a quarter of the chamber with a high resolution at the deposition surface (Fig. 2) using the mesh generator Gambit (Fluent Inc, Canonsburg, USA). First, the surface mesh at the deposition surface was created with triangular elements. The size of these elements increased linearly from the center toward the outlet boundary at a 1,500 μm radius from an edge with a length of 0.6 μm to 25 μm . Based on the surface mesh, four layers of prism cells were created with an aspect ratio of a tenth of the surface element size. The remaining volume was filled with tetrahedral elements. The largest element had an edge length of approximately 30 μm , so that the mesh consisted out of 2.8 Mio cells. To ensure the proper viscosity, the blood was modeled as an incompressible non-Newtonian fluid (Wellnhofer et al. 2010) with a density of 1,050 kg/m^3 and a hematocrit value of 40 %. Flow rates of 20, 40, and 80 ml/h were set

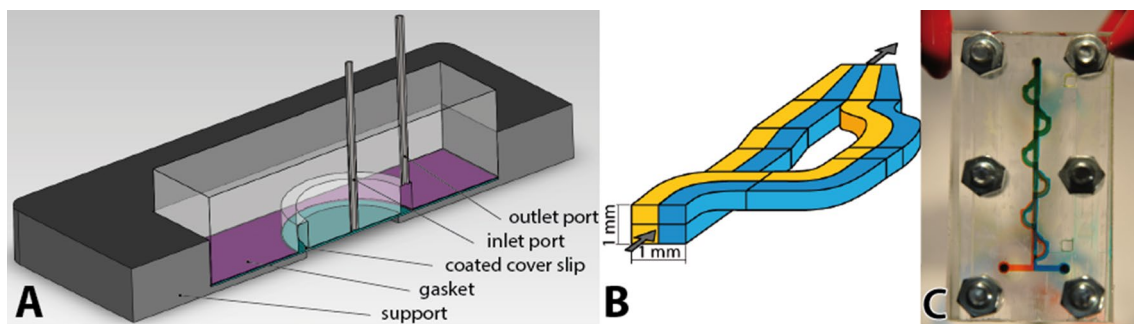
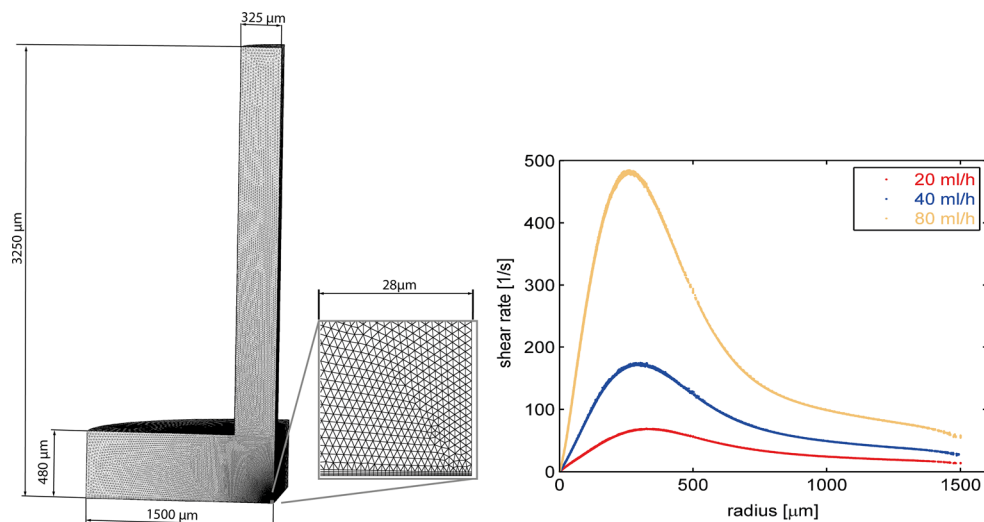


Fig. 1 Model of the flow chamber and laminar mixer. **a** The assembled stagnation point chamber consisting of a support, a coated glass cover slip, a silicon rubber gasket, and the top part. The silicon rubber has two functions: to create a seal between the cover glass and the top part and to create a 480- μm high gap. The top part possesses an inlet port at the center and an outlet port that is connected to the collecting annulus. **b** Principle of the laminar mixer. A fluid stream

enters the single stage and is divided into two streams (*top* and *bottom*) by a thin sheet (not shown). The top stream will be passed to the *right*; the height difference will then be evened out, and the inlet cross section will be restored. **c** The tested mixer and its functioning in the test setup. For better visualization, the streams are *colored* with *two colors* that show the mixing layer after the stage

Fig. 2 CFD model of the stagnation point flow chamber. A highly spatial resolved mesh (*left*) is generated for a quarter of the center of the chamber. The close-up image (*center*) presents the mesh of a symmetry plane at the stagnation point and illustrates the four boundary cell layers and the high resolution around the stagnation point. In a scatter plot (*right*), the WSS of each wall-adjacent numerical cell is plotted against the radial distance from the center of the chamber for 20, 40, and 80 ml/h flow rates



at the inlet, and a fully developed flow was assumed at the outlet. To verify the radial symmetric flow at the center, a coarser mesh simulation for the whole chamber—from the inlet to the outlet duct—was performed that also verified the peak shear rates of the described highly resolved mesh simulation. With a syringe pump (KDS Legato 210; KD Scientific Inc, Holliston, MA), the fluid was pulled from a blood reservoir through the chamber inlet, directed perpendicular to the cover slip, and collected in a 50-ml syringe (flow rates: 20, 40, and 80 ml/h; the corresponding peak shear rates were calculated via CFD simulation: 68, 173, and 480 s^{-1} ; Fig. 2). Before entering the flow chamber, the platelets were activated with a steady flow (ratio 1:10) of ADP (final concentration, 11.7 μM (Reininger et al. 1998); SERVA Electrophoresis GmbH, Heidelberg, Germany) supplied by a second syringe pump (Perfusor segura ft; B. Braun Melsungen AG, Melsungen, Germany). To ensure the rapid mixing of the two fluids, a serial multilamination mixer (Fig. 1a, b), which was described in detail by Schonfeld et al. (2004), was installed in front of the chamber. The experiments were performed at 37 °C.

Epifluorescence video microscopy was performed with a 10 \times objective (Plan Fluor, 10 \times /0.30, Ph1 DL, ∞ /1.2, WD 15.2; Nikon) to acquire videos using a CMOS Image Sensor FL-280 digital camera (ORCA[®]-flash 2.8; Hamamatsu Photonics Deutschland GmbH, Herrsching, Germany). The recording with the motorized stage and the joining of large images (3 \times 3 single images; final size of 1,795 \times 1,346 μm , spatial resolution of 0.72 $\mu m/px$) to videos (final frame rate of 0.24 fps) was automatically performed using the NIS-Elements [Ar 64-bit 3.20.00 (Build 677); Nikon] software. Illumination was provided by passing the output of a metal-halide lamp (X-Cite[®] 120PC; EXFO Life Science and Industrial Division, Mississauga,

Ontario, Canada) through a rhodamine band filter (G-1B, EX 546/10, DM 575, BA 590; Nikon).

All surfaces were perfused for at least 7 min. The data were normalized to the start of the ADP stimulation, prior to which hardly any platelet adhesion and no aggregation occurred. The typical circular deposits appeared around the center of the stagnation point (Fig. 3a).

2.3 Data analysis

The video data were analyzed using the NIS-Elements software with thresholding to mask the attached platelets and aggregates. The threshold was adjusted manually to fit the actual aggregate size when a bright corona due to high fluorescent signals encircled the growing aggregates (suppl. figure S1). An optimal threshold was achieved when a small variation of the value resulted in minor changes of the dividing line at the expected aggregate boundary. This process was performed for each image. From the start of the ADP stimulation, an image was appraised every 60 s using four criteria: the mean aggregate size, surface coverage, aggregate count, and probability of an embolic event. The mean and confidence interval were compared. The region of interest was the circle with a radius of 660 μm around the center of the stagnation point, that is, the site where the non-parallel flow substantially affects deposition.

The surface coverage was measured as the proportion of the area covered by platelet aggregates.

The probability of an embolic event was defined as the probability that at least one aggregate left the region of interest within this period of time and was analyzed for the total run of 7 min.

As described in Ono et al. (2008), the occurrence and intensity of platelet contraction was assessed by the observer. We

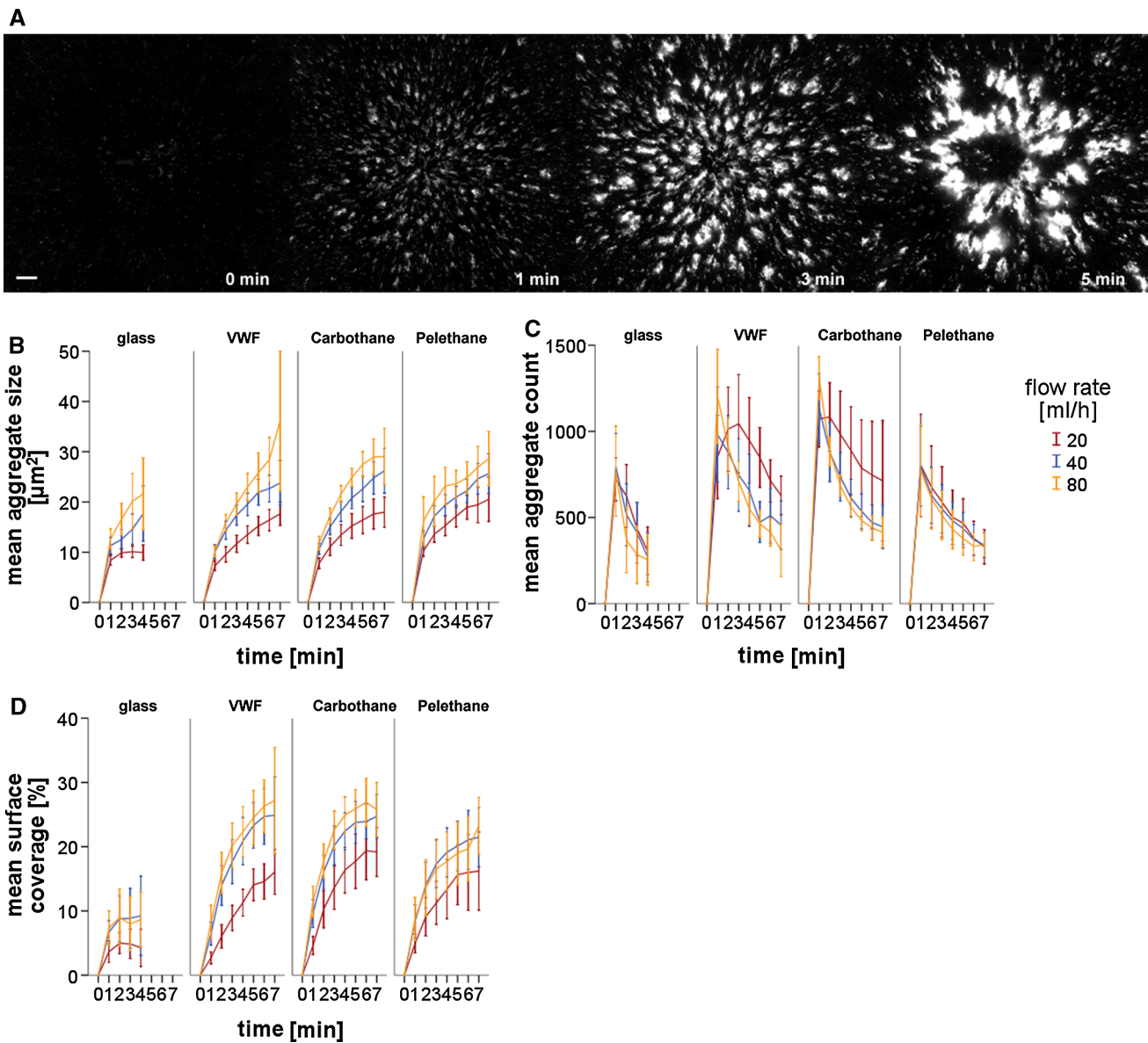


Fig. 3 Aggregate formation and growth on different surfaces. Whole blood ($n = 16$) is perfused over surfaces (glass, VWF, Carbothane, and Pellethane) at different flow rates (20, 40, and 80 ml/h) using ADP-stimulated platelets. Fluorescence microscopy of calcein-dyed platelets is performed with a $\times 10$ objective. The *error bars* indicate a 95 % confidence interval. **a** Representative video microscopy still images taken at a flow rate of 40 ml/h over the VWF surface. Beginning with few adherent platelets (0 min), the aggregates grew (1 + 3 min) in a typical pattern, which is symmetric around the stagnation point. With time (5 min), the aggregates began to embolize but

still increased in size. The *bar* represents 100 μm . **b** *Graphs* showing the mean aggregate size (μm^2) around the stagnation point over a time scale of 7 min for the different surfaces. Higher flow rates resulted in increased aggregate growth that is not linear to the flow rate. **c** The maximum of the mean aggregate count per image is a measurement of the thrombogenicity of the surface. **d** In contrast to the aggregate size, the increasing mean surface coverage (%) of the aggregates is dependent on the surface. Low flow rates (20 ml/h) are clearly offset, indicating a possible relationship with the changing fluid viscosity

defined four levels (Table 1) to evaluate the intensity of the aggregate contraction reaction (see also Fig. 5d, video S1).

Statistics were calculated using SPSS17 (IBM, Armonk, NY). Adobe Photoshop Pro CS3 and Adobe Premiere Pro CS3 (Adobe Systems Inc, San Jose, CA) were used for the image and video editing, respectively.

3 Results

In control experiments without platelet stimulation, no platelet deposition on the surface was observed; thus, the effects of the activation caused by the surface contact or shear during the mixing process can be neglected for the

Table 1 Intensity levels of aggregate contraction in stagnation point blood flow

Level	Description of intensity level
0	No or almost no contraction
1	Single aggregates contracting in a condensing manner
2	Multiple aggregates contracting into each other and combining into one large aggregate
3	The occurrence of extensive contraction of many aggregates or ring contraction

deposition results. When we tested different anticoagulants, the results were equivalent to the reported results in the present study.

3.1 Aggregate size, aggregate count, and surface coverage on different surfaces and flow rates

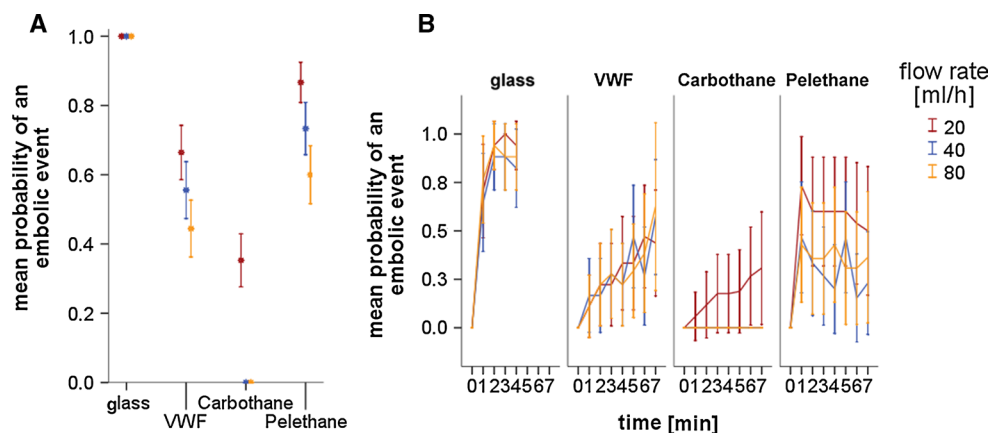
For all surfaces, the mean aggregate size depended of the flow rate. With increasing flow, the aggregates grew faster in the same time period, and this increase in aggregate growth was particularly prominent between the 20 and 40 ml/h flows. This difference was significant ($p < 0.05$) for three of the four surfaces (glass, VWF, and Carbothane), but no significance was obtained for the mean aggregate size between the 40 and 80 ml/h flows (Fig. 3b).

In contrast to the aggregate size, the mean aggregate count appeared to depend more on the perfused surface, although an additional flow effect could be observed. The aggregate count decreased steadily over time and was related to embolization and the coalescence of smaller aggregates into larger ones. On the glass and Pellethane surfaces, the platelets aggregated completely

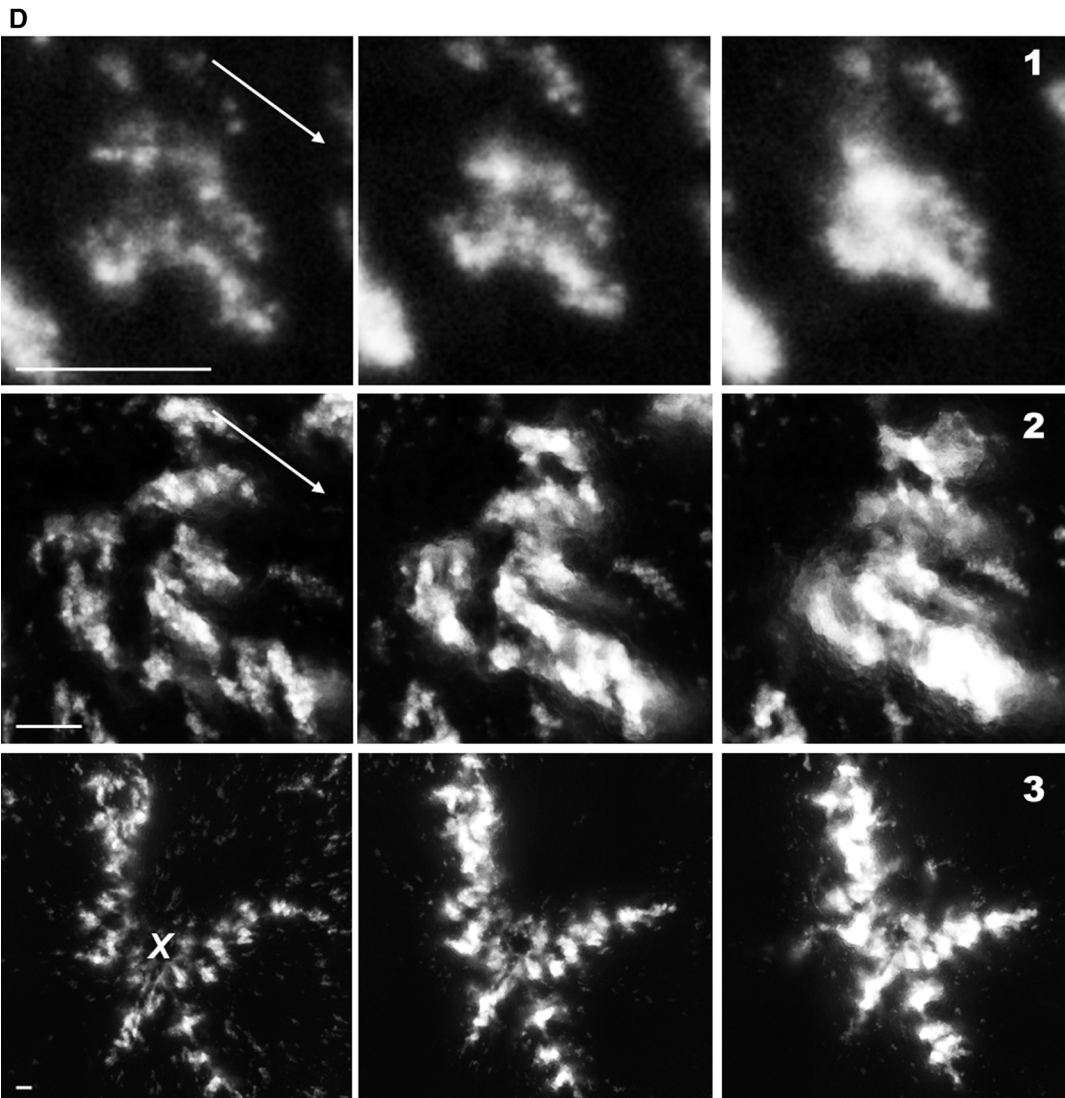
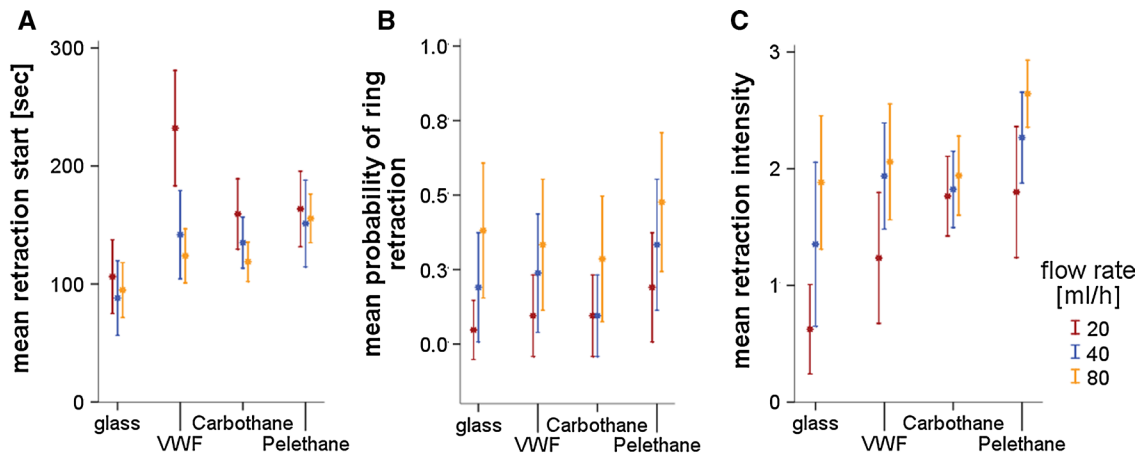
Fig. 5 Intensity of platelet contraction. Experiments, as described in Fig. 1, are further evaluated for platelet contraction. The error bars indicate a 95 % confidence interval. **a** Graph showing the mean time (s) when platelet contraction initiated. Small differences are observed between the flow rates. Contraction began on the glass surface first. The 20 ml/h experiments for the VWF outlier. **b** The formation of closed aggregate rings that subsequently retracted is more likely at a higher flow rate. **c** A scale from 0 to 3 is introduced to classify the mean contraction intensity of the aggregates on a specific surface and varied heavily between the surface and partly between the flow rates. **d** Representative video microscopy still images illustrating the contraction intensities 1 (upper row), 2 (middle row), and 3 (lower row), as described in Table 1. Images are acquired every 20–30 s. The flow direction is indicated by white arrows or the center of the stagnation point (white X, lower row) from which the fluid radiates symmetrically. The bars represent 50 μ m

independently of the flow rate, with Pellethane being more adhesive over time than glass. Even more aggregates were counted on the VWF and Carbothane surfaces, with both showing almost identical counts. The maximum count at 20 ml/h was lower and was not within the first minute of the experiments, but the values were higher throughout the experiments than those at 40 and 80 ml/h; although this difference can be observed in the graphs, the differences between the values were not significant ($p > 0.05$; Fig. 3c).

Last, the mean surface coverage was affected by both the flow rate and the surface. At 20 ml/h, the covered area was considerably smaller for all the surfaces, but the difference was only significant ($p < 0.05$) for VWF. The graphs for 40 and 80 ml/h were almost identical. In contrast to the aggregate size and count, the surface coverage appeared to reach a plateau phase after 7 min (Fig. 3d, also see video S2).

**Fig. 4** Aggregate embolization with different surfaces. Experiments, as described in Fig. 1, are further evaluated for embolization events. The error bars indicate a 95 % confidence interval. **a** Graph showing the mean probability of an embolization event for the individual surfaces

and flow rates. An embolization is more likely with a higher flow rate. **b** The mean probability of an embolization event over time is depicted for all the surfaces. Despite their differences, the surfaces had similar trends: Glass is similar to Pellethane, and VWF is similar to Carbothane



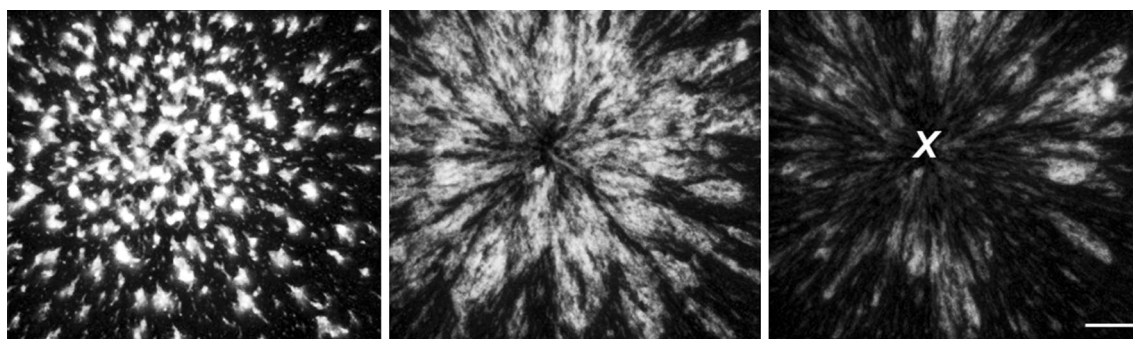


Fig. 6 Dissolving aggregates after halting ADP stimulation. After 10 min of the whole blood perfusion of a VWF-coated surface with ADP-stimulated platelets (*left*) at a flow rate 80 ml/h, the ADP inflow is terminated. The aggregates that grew around the stagnation point (white X) started to dissolve (*middle*; 1.5 min after ADT stop) and are

carried away by the flow almost completely within 3 min (*right*). The video microscopy still images are representative for all the surfaces and flow rates. Fluorescence microscopy of calcein-dyed platelets is performed with a $\times 10$ objective. The *bar* represents 200 μm

3.2 Probability of an embolic event with different surfaces and flow rates

Each surface showed a specific range for the probability of an embolic event at the tested flow rates (Fig. 4a), with decreasing probability in the following order: glass > Pellethane > VWF > Carbothane. Moreover, higher flow rates resulted in a reduced probability. The glass surface showed an extremely high rate of embolization; during the experiments, all the aggregates were embolized from the surface after 4–5 min. The opposite was found for the Carbothane coating: No embolization was observed, with the exception of a few experiments at the 20 ml/h flow rate. The aggregates were apparently stably adhered to the surface.

The temporal distribution revealed a different, more nuanced picture. The surface aggregates detached from the glass and Pellethane surfaces with similar probabilities during the entire experiment. In contrast, the probability increased continuously with the VWF coating, as well as for the 20 ml/h flow rate over the Carbothane surface (Fig. 4b).

3.3 Platelet contraction in stagnation point flow

Platelet adhesion and aggregation began with the ADP stimulation. Initially, the platelets were loosely aggregated to form a thrombus without clear boundaries. After several minutes of thrombus growth, the contraction began, as described previously (Ono et al. 2008); the complete aggregates tightened, and their boundaries became clear. More of the flowing platelets adhered and were pulled into the aggregate as if condensing on an interface. A dependency of the flow rate was observed according to the perfused surface: Contractions initiated earlier on the VWF and Carbothane surfaces with an increasing flow

rate, whereas there was a minimum initial time for the glass and Pellethane surfaces at 40 ml/h. For all the surfaces, the contraction began after approximately 2.5 min. The process initiated after 1.5 min only for the glass surface; the initiation time was 4 min at 20 ml/h for VWF (Fig. 5a).

In the course of a flow experiment, the growing aggregates formed a ring-like pattern around the center of the stagnation point (Fig. 3a, right images) (Reininger et al. 1998) that accumulated platelets and coalesced, most likely at a certain radial distance from the center of the stagnation point. This coalescing occurred directly on the surface or at a distance from the surface, such that a gap remained on the surface between the aggregates. When a ring was closed completely, it began to contract as one unit: The aggregates slid over the surface against the direction of the flow toward the center of the stagnation point. In general, this phenomenon was observed more frequently at higher flow rates; for all flow rates, the phenomenon appeared in <50 % of the experiments, and for the 20 ml/h experiments, it appeared in <12 %. This phenomenon was found with the Pellethane surface, with probabilities that were significantly higher: 70, 50, and 30 % for 80, 40, and 20 ml/h, respectively (Fig. 5b). This aggregate-retracting effect also occurred within a series of single aggregates outside the ring, causing the aggregates to merge into one compact aggregate.

The contraction intensity increased with increasing flow rate. Although the differences were small for the Carbothane surface, larger steps were observed for glass and Pellethane. The VWF surfaces showed only one step between 20 and 40 ml/h, and the Carbothane and VWF coatings had a relatively constant contraction reaction level of approximately 2 (see Table 1). The reaction range was lowest for glass and highest for Pellethane (Fig. 5c). When the ADP

flow for platelet stimulation was halted, the entire retracted aggregate formation dissolved; the aggregates gradually destabilized and were carried off in layers or as a whole by the flow (Fig. 6, video S3).

Ono et al. (2008) previously described the effect of platelet contraction in wall parallel flow over collagen type I, demonstrating its necessity for thrombus stability. In our experiments, we reproduced this phenomenon in a non-parallel flow situation, such as stagnation point flow on different artificial surfaces and flow velocities. The observed effect even led to a type of group dynamics involving several thrombi that were not previously described. Similar to Ono et al. we observed the reversibility of this process and therefore the dissolution of the thrombi.

3.4 Plasma protein-independent platelet adhesion and aggregation

A VWF coating represents a biological thrombogenic surface that naturally promotes platelet capture from the blood flow. The removal of the plasma proteins is expected to result in a lack of platelets adhering to the non-biological surfaces of glass and polyurethane. However, if the platelets had been directly bound to the surface without protein mediation, no aggregation should have been possible because no fibrinogen was present. Using washed platelets, all four surfaces showed extended platelet adhesion and aggregation in the described pattern. These aggregates were completely unstable; thus, the binding forces between the platelets and between the platelets and the surface were apparently weak. Platelet contraction was observable but never higher than the intensity of platelet contraction level 1 (see Table 1).

With a washed blood cell suspension as the fluid, the aggregate growth and embolization were found to be independent of the surface and distributed more evenly than those with whole blood. The greatest similarity with the previous experiments occurred on the VWF surface, whereas the glass surface appeared to be more thrombogenic without plasma proteins, and no passivation emerged. In contrast, both polyurethane surfaces showed weak adhesion (Fig. 7, video S4).

4 Discussion

Platelets that contact artificial materials may be activated due to shear, agonists (e.g., ADP), or the surface itself. These causes of platelet stimulation and thereby an increased disposition of adhesion and aggregation were stimulated using the steady inflow of ADP that was tested in previous experiments (Reininger et al. 1998); furthermore, we recently demonstrated that flow situations, such

as stagnation point flow, enhance platelet deposition (Reininger et al. 1993) and platelet–protein interaction (Kragh et al. 2014). Due to ADP stimulation, low calcium and magnesium levels do not hinder platelet activation and activity. Hence, the resulting apyrase inactivation provides steady ADP conditions and stimulation throughout the experiment (Jones et al. 2011). To evaluate the influence of flow and surfaces on platelet adhesion, aggregation, and embolization, we performed in vitro flow experiments using human whole blood with direct real-time observations.

As expected, the aggregates grew faster at higher flow rates because more platelets were transported to the site at the high velocity (Leiderman and Fogelson 2011). However, the increase in thrombus size was not proportional to the increase in the flow rates. Thus, other factors also played a role in thrombus growth rates (Kragh et al. 2014). Some researchers have proposed the idea of a ‘good wash out’ (Shu et al. 2009), which means that fewer platelets should deposit on surfaces in regions with a short blood residence time. We observed that the adhesion of aggregates on all the tested surfaces was weaker and less stable at lower flow rates. Thus, the probability of an embolic event for the total run was higher, and the surface coverage was lower. The recurring spacing between the 20 ml/h curve and the other two curves was particularly noticeable. An explanation may be found in the work of Hathcock (2006), who reported that the cell–cell interactions of red blood cells and other cells were greater than the adhesion forces of thrombocytes below wall shear rates of 100 s^{-1} . Additionally, aggregates are stabilized by plasma VWF only above 100 s^{-1} (Broos et al. 2011; Flamm and Diamond 2012). In our experiments, maximal shear rates over this threshold were reached at flow rates of 40 and 80 ml/h but not 20 ml/h, which is consistent with their findings.

The results demonstrate a connection between surface properties and the occurrence of microemboli alongside the flow velocity. These microemboli may depend on the strength of the thrombi’s adherence to the surface and the extent of its growth. Ideally, a surface should always be completely antithrombogenic. Nonetheless, in patients with mechanical circulatory support devices (MCSDs) (Thoenissen et al. 2005) or coronary bypass grafts (Clark et al. 1995), microembolizations are detected. In MCSD, the size of thrombi is limited by regular, short intervals of increased flow to remove the aggregates. This may be the cause for the emboli occurrence (John and Lee 2009). However, the number of microemboli is also increased in the case of coronary bypass grafts (Clark et al. 1995) but at physiological hemodynamics with a pulsatile flow without a forced wash-out cycle. Smaller aggregates consisting of only a couple of platelets disperse quickly in the blood current when they leave the site of stimulation and do not imply a general hemostatic issue (Loscalzo and Vaughan 1987). Similarly,

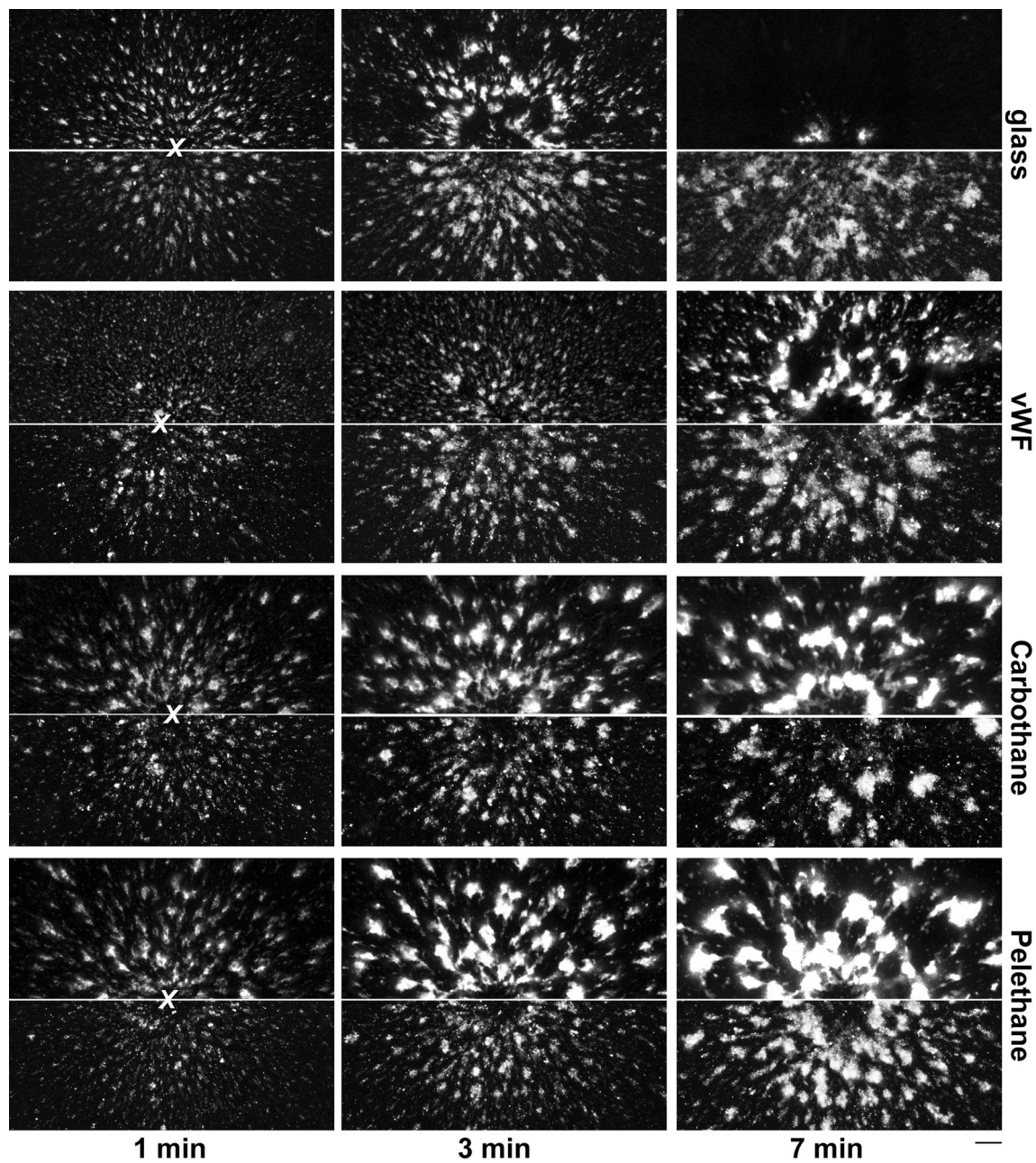


Fig. 7 Aggregate formation and embolization for different surfaces perfused with whole blood or washed blood. Whole blood ($n = 16$) or a washed blood cell suspension ($n = 3$) is perfused over surfaces (glass, VWF, Carbothane, and Pellethane) at a flow rate 40 ml/h with ADP-stimulated platelets. Representative half images (*upper part* whole blood; *lower part* washed blood) comparing the platelet adhesion, aggregation, and embolization after 1, 3, and 7 min of flow over

different surfaces (glass, VWF, Carbothane, and Pellethane). With the washed blood cell suspension, the manner of platelet aggregation is more independent of the surface than with the whole blood, but the aggregates are unstable. Fluorescence microscopy of calcein-dyed platelets is performed with a $\times 10$ objective. The white *X* indicates the center of the stagnation point, and the *bar* represents 100 μm

intensive aggregate growth does not necessarily result in the unsuitability of a surface, provided that the aggregates do not embolize into the vasculature or occlude the vessel. This possibility, for example, could lead to the better long-term integration of the artificial surface into the surrounding tissue (Garcia 2005). However, the characteristics of a

surface exposed to hemostatically active components from circulating blood may change over time. In most cases, adsorbed plasma proteins mediate the interaction of platelets with the surface. Due to the Vroman effect, an exchange of those proteins occurs, with the kinetics depending on the involved proteins, perfused surface, and possibly even the

flow (Hirsh et al. 2013; Leonard and Vroman 1991). Due to conformational changes during the process of adsorption or over time on a surface, the activity and functionality of proteins can be affected (Jung et al. 2013), suggesting that the detection of factors such as fibrinogen, VWF, and albumin using specific antibodies is not sufficient to identify the hemostatic relationships that actually exist in these boundary layers. Good results of minimizing platelet adhesion were obtained with antithrombotic surface coatings, such as heparin (Heise et al. 2006), or protein-repellent coatings (Zhang et al. 2009). However, in the harsh environment of blood flow, both the exchange of proteins and even the loss of functional groups on polymers can corrupt an artificial surface over time (Modic et al. 2012).

The maximum count of initially attaching aggregates within the first minutes of flow was a good measurement in our experiments to characterize the surface under flow conditions. This type of characterization was demanded by Ratner (2007) for decades. The thrombogenicity of a surface is important for hemostasis or rather, for the use of a surface in the blood stream; the thrombogenicity can be observed as the count of initially adhering platelets that form the seed of an aggregate. Over time, the aggregate count declined gradually due to embolization, platelet contraction, and the merging of aggregates. Furthermore, in clinical practice, it is crucial whether a formed thrombus adheres firmly to the surface or is carried away by the flow, possibly occluding smaller vessels. Therefore, a second important parameter is the probability of an embolization event over time that describes the strength of the surface–aggregate interface: Aggregates will embolize when the drag forces of the aggregates exceed the strength of the binding between the aggregates and the surface. Similarities and differences in these aspects could be observed for the four perfused surfaces in the present study. The adhesion and embolization differed considerably between both the polyurethane surfaces (Carbothane and Pellethane), whereas some analogies to the glass or the VWF coating, respectively, were found. Additionally, the glass surface was passivated to platelet adhesion after a couple of minutes of flow in most experiments, which was not the case with the other surfaces. However, at the higher flow rates, no embolization occurred with the Carbothane coating, although massive aggregate growth was detected.

The function performed by plasma proteins in platelet adhesion and aggregation was demonstrated in experiments with a washed blood cell suspension in which the plasma was replaced by Tyrode buffer containing albumin. Without fibrinogen or VWF, platelets should not be able to aggregate (Bang et al. 1972), and adhesion to non-biological surfaces—all the tested surfaces excluding the VWF coating—should be limited to some non-specific receptor interactions. The unexpected massive but unstable adhesion and

aggregation of platelets on all the tested surfaces confirmed the assumption that plasma proteins affect surface platelet interactions. The fact that such aggregations were observed in our experiments with the washed blood cell suspension was most likely due to VWF or similar hemostatically active proteins that are possibly released from the granules of stimulated platelets (Keenan and Solum 1972).

A further important finding is the characterization of the magnitude of platelet contraction. The platelet contraction, which led to a condensing effect of the aggregates, was enhanced by the flow. The mechanisms of platelet movement and thrombus contraction have been described previously (Brass et al. 2011; Lee et al. 2012; Morgenstern et al. 1984; Ono et al. 2008), and a general shear sensitivity of platelets under high shear stress has been demonstrated (Holme et al. 1997). However, the magnitude of platelet contraction, as we describe here, has not been revealed to date. For some surfaces and low flow rates, many small aggregates condensed into a larger thrombus, although it remains unclear whether this sliding over the surface loosened their adhesion to it, thereby increasing the embolic risk. Lam et al. (2011) measured the contraction force of a single adherent platelet and observed an increase in the force over time. Therefore, an earlier contraction motion would mean a lower strength of the surface binding, as we observed on glass. These characteristics correspond to a high probability of embolic events. For the other tested materials, embolic events were less probable, but the contraction time was higher. This finding indicates a stronger surface binding of the platelets. However, the stabilization of platelet aggregates by contraction has been shown (Ono et al. 2008) and was confirmed by our results, and we demonstrated the complete reversibility of this process when ADP stimulation was halted. However, further evidence is required to ascertain whether this effect also applies to other platelet agonists (Born 1962).

Many studies have been recently performed to investigate the kinetics (Satulovsky et al. 2000), exchange (Vogler 2012), amount (Claesson et al. 1995), and conformational changes (Moulin et al. 1999; Sadana 1992; Thakurta et al. 2012) of proteins adsorbed onto artificial surfaces. An active surface passivation through plasma proteins should be attempted in further materials research (Kador and Subramanian 2011). Many investigations were conducted with diverse plastic polymer surfaces and found different results, but all the studies used static systems for hemocompatibility observations (Li et al. 2013; Handa et al. 2014). These methods lack information about aggregate-forming processes and embolization. With this *in vitro* model, we provide a tool (Ratner 2007; Roest et al. 2011; Schaller et al. 2013) that can characterize surfaces under defined, non-parallel blood flow conditions. If the basic concept is known, the experimental time can be extended to meet the

requirements of general hemocompatibility issues. While the present model provides no evidence of the underlying mechanisms, the linkage of artificial surfaces and direct, real-time platelet activity observations over time offers the determination of platelet attachments and embolization events and will expand investigations on hemocompatibility. This *in vitro* model forms the basis for new experimental studies to improve the care of patients who have artificial devices. The efficacy of ADP-receptor-directed medication could also be compared with traditional measurements.

Acknowledgments The authors thank their colleagues from the thrombocyte transfusion service from the Department of Transfusion Medicine of the Medical Center of the University of Munich for their kind help with the blood collection. This work was supported by the German Research Foundation (DFG) [Grant Number GZ: RE 1293/5—1].

Conflict of interest None.

References

- Arjun GN, Ramesh P (2012) Structural characterization, mechanical properties, and *in vitro* cytocompatibility evaluation of fibrous polycarbonate urethane membranes for biomedical applications. *J Biomed Mater Res A* 100A(11):3042–3050
- Backes D, van den Bergh WM, van Duijn AL, Lahpor JR, van Dijk D, Slooter AJC (2012) Cerebrovascular complications of left ventricular assist devices. *Eur J Cardiothorac Surg* 42(4):612–620
- Bang NU, Trygstad CW, Heiden R (1972) Plasma-protein requirements for human platelet aggregation. *Ann NY Acad Sci* 201:280
- Beiras-Fernandez A, Kanzler I, Michel S, Sadoni S, Kilger E, Beiras A, Kur F (2013) Platelet factor 4-positive thrombi adhering to the ventricles of a ventricular assist device in patients with heparin-induced thrombocytopenia type II. *Transplant Proc* 45(5):2013–2016
- Born GVR (1962) Aggregation of blood platelets by adenosine diphosphate and its reversal. *Nature* 194(4832):927
- Brass LF, Wannemacher KM, Ma P, Stalker TJ (2011) Regulating thrombus growth and stability to achieve an optimal response to injury. *J Thromb Haemost* 9:66–75
- Broos K, Feys HB, De Meyer SF, Vanhoorelbeke K, Deckmyn H (2011) Platelets at work in primary hemostasis. *Blood Rev* 25(4):155–167
- Claesson PM, Blomberg E, Froberg JC, Nylander T, Arnebrant T (1995) Protein interactions at solid-surfaces. *Adv Colloid Interface Sci* 57:161–227
- Clark RE, Brillman J, Davis DA, Lovell MR, Price TRP, Magovern GJ (1995) Microemboli during coronary-artery bypass-grafting—genesis and effect an outcome. *J Thorac Cardiovasc Surg* 109(2):249–258
- Colace TV, Tormoen GW, McCarty OJT, Diamond SL (2013) Microfluidics and coagulation biology. *Annu Rev Biomed Eng* 15:283–303
- Fare S, Valtulina V, Petrini P, Alessandrini E, Pietrocola G, Tanzi MC, Speziale P, Visai L (2005) *In vitro* interaction of human fibroblasts and platelets with a shape-memory polyurethane. *J Biomed Mater Res A* 73A(1):1–11
- Flamm MH, Diamond SL (2012) Multiscale systems biology and physics of thrombosis under flow. *Ann Biomed Eng* 40(11):2355–2364
- Garcia AJ (2005) Get a grip: integrins in cell-biomaterial interactions. *Biomaterials* 26(36):7525–7529
- Handa H, Major TC, Brisbois EJ, Amoako KA, Meyerhoff ME, Bartlett RH (2014) Hemocompatibility comparison of biomedical grade polymers using rabbit thrombogenicity model for preparing nonthrombogenic nitric oxide releasing surfaces. *J Mater Chem B* 2(8):1059–1067
- Hathcock JJ (2006) Flow effects on coagulation and thrombosis. *Arterioscler Thromb Vasc Biol* 26(8):1729–1737
- Heise M, Schmidmaier G, Husmann I, Heidenhain C, Schmidt J, Neuhaus P, Settmacher U (2006) PEG-hirudin/iloprost coating of small diameter ePTFE grafts effectively prevents pseudointima and intimal hyperplasia development. *Eur J Vasc Endovasc Surg* 32(4):418–424
- Hirsh SL, McKenzie DR, Nosworthy NJ, Denman JA, Sezeran OU, Bilek MMM (2013) The vroman effect: competitive protein exchange with dynamic multilayer protein aggregates. *Colloids Surf B Biointerfaces* 103:395–404
- Holme PA, Orvim U, Hamers M, Solum NO, Brosstad FR, Barstad RM, Sakariassen KS (1997) Shear-induced platelet activation and platelet microparticle formation at blood flow conditions as in arteries with a severe stenosis. *Arterioscler Thromb Vasc Biol* 17(4):646–653
- Horbett TA (1993) Principles underlying the role of adsorbed plasma-proteins in blood interactions with foreign materials. *Cardiovasc Pathol* 2(3):137–148
- John R, Lee S (2009) The biological basis of thrombosis and bleeding in patients with ventricular assist devices. *J Cardiovasc Transl Res* 2(1):63–70
- Jones S, Evans RJ, Mahaut-Smith MP (2011) Extracellular Ca²⁺ modulates ADP-evoked aggregation through altered agonist degradation: implications for conditions used to study P2Y receptor activation. *Br J Haematol* 153(1):83–91
- Jung F, Braune S, Lendlein A (2013) Haemocompatibility testing of biomaterials using human platelets. *Clin Hemorheol Microcirc* 53:97–115
- Kador KE, Subramanian A (2011) Surface modification of biomedical grade polyurethane to enable the ordered co-immobilization of two proteins. *J Biomater Sci Polym Ed* 22(15):1983–1999
- Keenan JP, Solum NO (1972) Quantitative studies on release of platelet fibrinogen by thrombin. *Br J Haematol* 23(4):461
- Kragh T, Napoleone M, Fallah MA, Gritsch H, Schneider MF, Reininger AJ (2014) High shear dependent von Willebrand factor self-assembly fostered by platelet interaction and controlled by ADAMTS13. *Thromb Res* 133(6):1079–1087
- Krajewski S, Krauss S, Kurz J, Neumann B, Schlenk C, Wendel HP (2014) Real-time measurement of free thrombin: evaluation of the usability of a new thrombin assay for coagulation monitoring during extracorporeal circulation. *Thromb Res* 133(3):455–463
- Kuettling M, Roggenkamp J, Urban U, Schmitz-Rode T, Steinseifer U (2011) Polyurethane heart valves: past, present and future. *Expert Rev Med Devices* 8(2):227–233
- Lam WA, Chaudhuri O, Crow A, Webster KD, Li T-D, Kita A, Huang J, Fletcher DA (2011) Mechanics and contraction dynamics of single platelets and implications for clot stiffening. *Nat Mater* 10(1):61–66
- Lee D, Fong KP, King MR, Brass LF, Hammer DA (2012) Differential dynamics of platelet contact and spreading. *Biophys J* 102(3):472–482
- Leiderman K, Fogelson AL (2011) Grow with the flow: a spatial-temporal model of platelet deposition and blood coagulation under flow. *Math Med Biol* 28(1):47–84
- Leonard EF, Vroman L (1991) Is the Vroman effect of importance in the interaction of blood with artificial materials. *J Biomater Sci Polym Ed* 3(1):95–107

- Li P, Cai X, Wang D, Chen S, Yuan J, Li L, Shen J (2013) Hemocompatibility and anti-biofouling property improvement of poly(ethylene terephthalate) via self-polymerization of dopamine and covalent graft of zwitterionic cysteine. *Colloids Surf B Biointerfaces* 110:327–332
- Loscalzo J, Vaughan DE (1987) Tissue plasminogen-activator promotes platelet disaggregation in plasma. *J Clin Investig* 79(6):1749–1755
- Modic M, Junkar I, Vesel A, Mozetic M (2012) Aging of plasma treated surfaces and their effects on platelet adhesion and activation. *Surf Coat Technol* 213:98–104
- Morgenstern E, Korell U, Richter J (1984) Platelets and fibrin strands during clot retraction. *Thromb Res* 33(6):617–623
- Moulin AM, O’Shea SJ, Badley RA, Doyle P, Welland ME (1999) Measuring surface-induced conformational changes in proteins. *Langmuir* 15(26):8776–8779
- Neves KB, Onasoga AA, Wufsus AR (2013) The use of microfluidics in hemostasis: clinical diagnostics and biomimetic models of vascular injury. *Curr Opin Hematol* 20(5):417–423
- Oono A, Westein E, Hsiao S, Nesbitt WS, Hamilton JR, Schoenwaelder SM, Jackson SP (2008) Identification of a fibrin-independent platelet contractile mechanism regulating primary hemostasis and thrombus growth. *Blood* 112(1):90–99
- Ratner BD (2007) The catastrophe revisited: blood compatibility in the 21st century. *Biomaterials* 28(34):5144–5147
- Reininger AJ, Reininger CB, Wurzing LJ (1993) The influence of fluid-dynamics upon adhesion of ADP-stimulated human platelets to endothelial-cells. *Thromb Res* 71(3):245–249
- Reininger AJ, Korndorfer MA, Wurzing LJ (1998) Adhesion of ADP-activated platelets to intact endothelium under stagnation point flow in vitro is mediated by the integrin alpha IIb beta 3. *Thromb Haemost* 79(5):998–1003
- Reininger AJ, Agneskirchner J, Bode PA, Spannagl M, Wurzing LJ (2000) C7E3 Fab inhibits low shear flow modulated platelet adhesion to endothelium and surface-adsorbed fibrinogen by blocking platelet GP IIb/IIIa as well as endothelial vitronectin receptor—results from patients with acute myocardial infarction and healthy controls. *Thromb Haemost* 83(2):217–223
- Roest M, Reininger A, Zwaginga JJ, King MR, Heemskerk JWM (2011) Flow chamber-based assays to measure thrombus formation in vitro: requirements for standardization. *J Thromb Haemost* 9(11):2322–2324
- Ruggeri ZM, Orje JN, Habermann R, Federici AB, Reininger AJ (2006) Activation-independent platelet adhesion and aggregation under elevated shear stress. *Blood* 108(6):1903–1910
- Sadana A (1992) Protein adsorption and inactivation on surfaces— influence of heterogeneities. *Chem Rev* 92(8):1799–1818
- Satulovsky J, Carignano MA, Szleifer I (2000) Kinetic and thermodynamic control of protein adsorption. *Proc Nat Acad Sci USA* 97(16):9037–9041
- Schaller J, Kragh T, Reininger A, Goubergrits L, Kertzsch U, Spannagl M, Affeld K (2013) Biocompatibility material test for cardiovascular devices using stagnation point flow. *Biomed Tech* 58:3
- Schonfeld F, Hessel V, Hofmann C (2004) An optimised split-and-recombine micro-mixer with uniform ‘chaotic’ mixing. *Lab Chip* 4(1):65–69
- Shin IG, Kim DG, Kim HK, Kim SH, Jeon DM, Suh TS, Jang HS (2012) Development of drug eluting stent for the treatment of benign biliary stricture by electro-spray method. *Polym Korea* 36(2):163–168
- Shu F, Parks R, Maholtz J, Ash S, Antaki JF (2009) Multimodal flow visualization and optimization of pneumatic blood pump for sorbent hemodialysis system. *Artif Organs* 33(4):334–345
- Thakurta SG, Miller R, Subramanian A (2012) Adherence of platelets to in situ albumin-binding surfaces under flow conditions: role of surface-adsorbed albumin. *Biomed Mater* 7(4):1–10
- Thoenissen NH, Schneider M, Allroggen A, Ritter MT, Dittrich R, Schmid C, Scheld HH, Ringelstein EB, Nabavi DG (2005) High level of cerebral microembolization in patients supported with the DeBakey left ventricular assist device. *J Thorac Cardiovasc Surg* 130(4):1159–1166
- Trigwell S, De S, Sharma R, Mazumder MK, Mehta JL (2006) Structural evaluation of radially expandable cardiovascular stents encased in a polyurethane film. *J Biomed Mater Res B Appl Biomater* 76B(2):241–250
- van Oeveren W, Tielliu IF, de Hart J (2012) Comparison of modified Chandler, roller pump, and ball valve circulation models for in vitro testing in high blood flow conditions: application in thrombogenicity testing of different materials for vascular applications. *Int J Biomater* 2012:673163
- Vermette P, Griesser H, Laroche G, Guidoin R (2001) Biomedical applications of polyurethanes. *Landes Bioscience, Georgetown*
- Versteeg HH, Heemskerk JWM, Levi M, Reitsma PH (2013) New fundamentals in hemostasis. *Physiol Rev* 93(1):327–358
- Vogler EA (2012) Protein adsorption in three dimensions. *Biomaterials* 33(5):1201–1237
- Wellenhofer E, Osman J, Kertzsch U, Affeld K, Fleck E, Goubergrits L (2010) Flow simulation studies in coronary arteries—impact of side-branches. *Atherosclerosis* 213(2):475–481
- Westein E, de Witt S, Lamers M, Cosemans JMEM, Heemskerk JWM (2012) Monitoring in vitro thrombus formation with novel microfluidic devices. *Platelets* 23(7):501–509
- Zhang X, Halvorsen K, Zhang C-Z, Wong WP, Springer TA (2009) Mechanoenzymatic cleavage of the ultralarge vascular protein von Willebrand factor. *Science* 324(5932):1330–1334